NOAA Technical Report NESDIS 39

General Determination of Earth Surface Type and Cloud Amount Using Multispectral AVHRR Data

Washington, D.C.
February 1988

U.S. DEPARTMENT OF COMMERCE
National Oceanic and Atmospheric Administration
National Environmental Satellite, Data, and Information Service

NOAA TECHNICAL REPORTS

National Environmental Satellite, Data, and Information Service

Environmental Satellite, Data, and Information Service (NESDIS) manages the Nation's civil atellite systems, as well as global national data bases for meteorology, oceanography, geophysics, and solar-terrestrial sciences. From these sources, it develops and disseminates environmental data and information products critical to the protection of life and property, national defense, the national economy, energy development and distribution, global food supplies, and the development of natural resources.

Publication in the NOAA Technical Report series does not preclude later publication in scientific journals in expanded or modified form. The NESDIS series of NOAA Technical Reports is a continuation of the former NESS and EDIS series of NOAA Technical Reports and the NESC and EDS series of Environmental Science Services Administration (ESSA) Technical Reports.

These reports are available from the National Technical Information Service (NTIS), U.S. Department of Commerce, Sills Bldg., 5285 Port Royal Road, Springfield, VA 22161 (prices on request for paper copies or microfiche, please refer to PB number when ordering) or by contacting Nancy Everson, NOAA/NESDIS, 5200 Auth Road, Washington, DC 20233 (when extra copies are available). A partial listing of more recent reports appear below:

NESDIS SERIES

NESDIS 1 Satellite Observations on Variations in Southern Hemisphere Snow Cover. Kenneth F. Dewey and Richard Heim, Jr., June 1983. (PB83 252908)

NESDIS 2 NODC 1 An Environmental Guide to Ocean Thermal Energy Conversion (OTEC) Operations in the Gulf of Mexico. National Oceanographic Data Center, June 1983. (PB84 115146)

NESDIS 3 Determination of the Planetary Radiation Budget from TIROS-N Satellites. Arnold Gruber, Irwin Ruff and Charles Earnest, August 1983. (PB84 100916)

NESDIS 4 Some Applications of Satellite Radiation Observations to Climate Studies. T.S. Chen, George Ohring and Haim Ganot, September 1983. (PB84 108109)

NESDIS 5 A Statistical Technique for Forecasting Severe Weather from Vertical Soundings by Satellite and Radiosonde. David L. Keller and William L. Smith, June 1983. (PB84 114099)

NESDIS 6 Spatial and Temporal Distribution of Northern Hemisphere Snow Cover. Burt J. Morse and Chester F. Ropelewski (NWS), October 1983. (PB84 118348)

NESDIS 7 Fire Detection Using the NOAA--Series Satellites. Michael Matson, Stanley R. Schneider, Billie Aldridge and Barry Satchwell (NWS), January 1984. (PB84 176890)

NESDIS 8 Monitoring of Long Waves in the Eastern Equatorial Pacific 1981-83 Using Satellite Multi-Channel Sea Surface Temperature Charts. Richard Legeckis and William Pichel, April 1984. (PB84 190487)

NESDIS 9 The NESDIS-SEL Lear Aircraft Instruments and Data Recording System. Gilbert R. Smith, Kenneth O. Hayes, John S. Knoll and Robert S. Koyanagi, June 1984. (PB84 219674)

NESDIS 10 Atlas of Reflectance Patterns for Uniform Earth and Cloud Surfaces (NIMBUS-7 ERB--61 Days). V.R. Taylor and L.L. Stowe,July 1984. (PB85 12440)

NESDIS 11 Tropical Cyclone Intensity Analysis Using Satellite Data. Vernon F. Dvorak, September 1984. PB85 112951)

NESDIS 12 Utilization of the Polar Platform of NASA's Space Station Program for Operational Earth Observations. John H. McElroy and Stanley R. Schneider, September 1984. (PB85 1525027AS)

NOAA Technical Report NESDIS 39

General Determination of Earth Surface Type and Cloud Amount Using Multispectral AVHRR Data

Irwin Ruff and Arnold Gruber
Satellite Research Laboratory
Washington, D.C. 20233

U.S. DEPARTMENT OF COMMERCE
C. William Verity, Secretary

National Oceanic and Atmospheric Administration
J. Curtis Mack II, Assistant Secretary

National Environmental Satellite, Data, and Information Service
Thomas N. Pyke, Jr., Assistant Administrator

Contents

Tables

General Determination of Earth Surface Type and Cloud Amount Using Multispectral AVHRR Data

Irwin Ruff and Arnold Gruber
National Oceanic and Atmospheric Administration
National Environmental Satellite,Data, and Information Service
Satellite Research Laboratory
Washington, D.C., 20233

Abstract

A method is presented for determining the type of daylight scene viewed by every resolution element of AVHRR for routine, large-scale processing, using mainly values from the various spectral channels of AVHRR. The specification of scene types was restricted to the broad catagories of vegetation, non-vegetated land, water, snow/ice and cloud. The method appears to be sufficiently sensitive, however, to permit it to be extended to finer specification of scene type.

1. Introduction

The components of the Earth's radiation budget have been computed from satellite data for many years, although lack of information has forced a number of simplifying assumptions. Two of these assumptions may now be replaced by empirical models of bi-directional and directional reflection for various combinations of natural surfaces and clouds (e.g.,Suttles et al, 1988). However, to apply these models correctly, it is necessary to know the type of surface being observed, at least in a general sense.

Much work has been done on scene identification from satellites, both with LANDSAT and with AVHRR. Early examples of such studies are Rouse et al, 1974 and Gray and McCrary, 1981. These studies have dealt with comparatively small amounts of data and limited areas, where the nature of the surface and at least the general type of vegetation are known *a priori*. Under these conditions the identification methods used have proved to be very sensitive, e.g., distinguishing between different crops, or determining the degree of drought.

For purposes of observing the components of the radiation budget for the entire Earth, however, the requirements are on a totally different scale. AVHRR provides information for approximately 35 million separate daylight locations in the course of one day. A scene identification method that is to be used for routine processing of this data must thus be completely objective, and be able to evaluate any set of conditions that may be encountered any place on Earth, at any time of year. Operational constraints also limit the complexity of such an algorithm.

One possible approach would be to prepare a detailed table of surface type for the entire Earth. While theoretically possible, the large size of such a table at the resolution required, as well as the necessity of accounting for seasonal changes make this approach unwieldy in practice. Further, it would still be necessary to determine the amount of cloud or of snow/ice present in a scene. The aim of this study was therefore to identify the Earth surface type and the cloud amount within single observational fields of AVHRR, using, as far as possible, only information available from that instrument.

2. Instrument and Data

AVHRR is a multi-spectral cross track scanner mounted on the TIROS-N series of satellites, with a scan rate of six scans per second. Although the instantaneous field of view, called a Local Area Coverage (LAC) spot, is about 1 km ground resolution at nadir, the data is not usually used in this form, except for special studies. Groups of four out of five fields of view along a scan line are combined to form a lower resolution element, termed a Global Area Coverage (GAC) spot. This is done for only every third scan. The relationships of these resolution elements are shown in Fig. 1.

There are either four or five spectral channels, depending on the instrument model. The nominal wavelength intervals are given in Table 1, and Fig. 2 shows the normalized respense functions along with the spectral distributions of the incident solar energy and the energy emitted from a 300°K blackbody. It may be seen that channels 1 and 2 will observe reflected solar energy in the red portion of the visible and in the near infrared, respectively, while channels 4 and 5 will observe emitted terrestrial energy in the 10-12 μm window. (Channel 5 is missing on four channel instruments.) At the wavelength of channel 3, centered at about 3.7 μm, both solar and terrestrial radiation are of importance. The implications of this will be discussed in detail below.

Table 1

Channel	Wavelength
1	.58 to .68 μm
2	.725 to 1.1 μm
3	3.55 to 3.93 μm
4	10.3 to 11.3 μm
5	11.5 to 12.5 μm

Two sets of GAC data were stored on disc, comprising three complete orbits from NOAA 6 on 13 April, 1981 and three orbits from NOAA 7 on 26 August, 1981. For both sets the daylight portions extend from Africa and Europe westward across the Atlantic Ocean and include some of the Americas, making available a wide variety of scene types for study. Since NOAA 6 had a 0730 local time descending node while NOAA 7 had a 1430 local time ascending node, the first data set represented conditions for a low morning sun, while the second set was observed with a high afternoon sun. This permitted an evaluation of the effects of solar zenith angle. The only ground truth available for this data other than large scale geographic information and normal mereorological observations was visible and infra-red images of the satellite data.

3. Treatment of Channel 3

The daylight measurements from channel 3 are difficult to interpret since this channel will sense both reflected solar and emitted terrestrial radiation (see Fig. 2). In order to make use of these measurements, it is necessary to know the magnitudes of the two components. What has heretofore been used as an indicator of the magnitude of the reflected component has been the difference between the channel 3 and channel 4 temperatures. As will be shown below this difference is not conservative, since it may result from varying physical conditions. Additionally, it is difficult to compare a temperature difference directly with any other quantity measured by AVHRR.

To resolve this problem reflectivities were calculated for channel 3 using a method in which the assumptions and procedure were clearly defined. In view of the uncertainties in observations at 3.7 μm, it is doubtful that any such method will yield absolute values. However, the results should be internally consistant, and might be related to the reflectivities from channels 1 and 2 (with which they can now directly be compared) in a coherent manner.

The main assumption is the same as that implicit in the use of the temperature difference between channels 3 and 4, i.e., that the radiation temperature at channel 3 wavelengths is given by the observed channel 4 temperature. This assumption is poor. Variations in such things as emissivity or in atmospheric transmission between the two wavelengths assure that the temperature differences will not only not be zero, but that they will vary greatly. The practical influence of this assumption on the effectiveness of the method can be shown only after it is applied to the test data.

Let T be the body temperature of the surface,(assumed equal to the channel 4 equivalent black-body temperature), T_3 the observed channel 3 temperature, λ the wavelength in micrometers, $f(\lambda)$ the channel 3 wavelength response, $S(\lambda)$ the incident solar energy, ζ the solar zenith angle at the observed point, ε the mean emissivity and r the mean reflectivity of the surface for channel 3 wavelengths. The emitted flux in watts/meter^2/μm is given by the Plank function,

$$P(T,\lambda) = C_1 \lambda^{-5} \left[e^{C2/\lambda T} -1 \right]^{-1} \qquad (1)$$

where $C = 3.7515 \times 10^{8}$ w $\mu m^{2} \mu^{-1}$ and $C = 14388.33$ μm deg.

It is then possible to write

$$\int_0^\infty P(T_s,\lambda) f(\lambda) d\lambda = \varepsilon \int_0^\infty P(T,\lambda) f(\lambda) d\lambda + r \cos\zeta \int_0^\infty S(\lambda) f(\lambda) d\lambda \qquad (2)$$

If the transmissivity of the surface is negligible, then

$$\varepsilon + r = 1 \qquad (3)$$

This assumption is reasonable for almost all surfaces at 3.7 μm including water (Wolfe and Zissis, 1978). One case for which this is not true is an optically thin cloud. However, for such a situation, radiation from the Earth's surface will also penetrate the cloud and reach the satellite. It is thus possible to view this as a composite surface type for which the total transmissivity is zero.

Combining equations (2) and (3),

$$r = \frac{\int P(T_s,\lambda)\ f(\lambda)\ d\lambda - \int_0^\infty P(T,\lambda)\ f(\lambda)\ d\lambda}{\cos\zeta \int_0^\infty S(\lambda)\ f(\lambda)\ d\lambda - \int_0^\infty P(T,\lambda)\ f(\lambda)\ d\lambda} \qquad (4)$$

It is obvious that r cannot be determined in the absence of solar illumination. However, this is also true when the incident solar energy is greater than zero, but small. It may be seen from equations (2) and (3) that the limiting case occurs when $\cos\zeta \int_0^\infty S(\lambda)\ f(\lambda)\ d\lambda = \int_0^\infty P(T,\lambda)\ f(\lambda)\ d\lambda$,

at which point, $\int_0^\infty P(T_s,\lambda)\ f(\lambda)\ d\lambda = \int_0^\infty P(T,\lambda)\ f(\lambda)\ d\lambda$,

This limit is given by

$$\cos\zeta_{lim} = \frac{\int_0^\infty P(T,\lambda)\ f(\lambda)\ d\lambda}{\int_0^\infty S(\lambda)\ f(\lambda)\ d\lambda} \qquad (5)$$

Only when the solar zenith angle is less than ζ_{lim} is it possible to distinguish between emitted and reflected components, and to make an estimate of reflectivity. This function is shown in Fig. 3.

As long as $\zeta < \zeta_{lim}$, it is impossible for T_3 to be less than T_4. (At terrestrial temperatures the emitted energy for channel 3 will of course always be much less than for channel 4.) If the emissivities for channels 3 and 4 are actually both equal to 1, the observed temperatures would be the same in the absence of atmospheric effects. Since the atmospheric transmissivity is greater for channel 3 than for channel 4, T_3 will be observed as greater than T_4. If the channel 4 emissivity should not be equal to 1, and the channel 3 emissivity be greater, clearly T_3 will be greater than T_4. The third possible case is if the channel 3 emissivity is less than that of channel 4. In this case, the emitted component would result in a channel 3 temperature lower than that of channel 4. However, from equation (3), as the emissivity decreases, the reflectivity increases, and as long as $\zeta < \zeta_{lim}$,

$$\cos\zeta \int_0^\infty S(\lambda)\, f(\lambda)\, d\lambda \;>\; \int_0^\infty P(T,\lambda)\, f(\lambda)\, d\lambda .$$

This condition thus results in the outgoing energy in channel 3 being greater than if the emissivity were equal to 1.

There are, however, a large number of observations where ζ is much less than ζ_{lim} but where the channel 3 temperature is lower than that of channel 4, often by several degrees. Since this should be impossible, some explanation must be sought.

Although measurements of reflection from natural surfaces in the 3.7 μm region are lacking, there is no reason to believe that such reflection would not exhibit the angular variations seen in the visible, although the patterns might be slightly different due to the longer wavelength. It is thus quite possible that in cases where $T_3 < T_4$, all or most of the incident solar radiation is being reflected in a direction other than that viewed by the satellite. Of course such angular dependence is not a function of viewing angle, and even when $T_3 < T_4$ the reflected component seen by the satellite may not be representative of the reflected energy over the entire upward hemisphere, any more than is the case with channels 1 or 2.

In order to obtain some estimate of the channel 3 reflectivity when $T_3 < T_4$, it was assumed that all reflected solar energy is in other than the viewed direction. Consequently only emitted energy is measured. Then from equations (2) and (3),

$$r = 1 - \frac{\int_0^\infty P(T_3,\lambda)\ f(\lambda)\ d\lambda}{\int_0^\infty P(T,\lambda)\ f(\lambda)\ d\lambda} \qquad (6)$$

The relationship between reflectivities calculated when $T_3 > T_4$ and the temperature difference between channels 3 and 4 is illustrated in Fig. 4 for a solar zenith angle of 0°. The assumption that the body temperature for channel 3 is equal to T_4 implies that if T_3 and T_4 are both fixed, the reflected energy in channel 3 is also fixed. However, from equation (4), the resultant channel 3 reflectivity will increase as the secant of the solar zenith angle. This is simple to take into account. If both temperatures are increased by the same amount, T_3-T_4 remains unchanged, but the reflected energy, and hence the channel 3 reflectivity increases. Thus, any given temperature difference may be due to very different physical conditions. It appears preferable, therefore, to use calculated channel 3 reflectivities rather than values of $T_3 - T_4$, in spite of uncertainties involved in the calculation of the first quantity.

The main uncertainty is the effect of assuming that the radiation temperature for channel 3 is identical with the observed channel 4 temperature. To investigate this, distributions of the channel 3 - channel 4 temperature difference were examined using only nighttime observations from the test data set. In every area there was a wide range of differences. One area, which had the maximum difference (almost 25°) was examined further. A regression of T_3-T_4 against T_4 was fitted to the data of this area, resulting, as would be expected, in a definite overall improvement in the predicted value of T_3. However, the maximum difference between predicted and observed values of T_3 was still greater than 16°. When a similar regression line was calculated by combining the data from all the geographic areas and applied to this single area, the overall errors were worse than for the assumption that the channel 3 temperature was equal to that of channel 4. It thus appears that for large-scale data processing, the best approximation to the channel 3 temperature is the channel 4 temperature, unless information is available regarding the type of area being viewed. Since the purpose of this estimate is to identify the observed scene, this will not be the case.

In order to estimate the distribution of errors in the channel 3 reflectivity that would result from the channel 3 temperature not being equal to that of channel 4, the nighttime data for the single geographic area considered above was assumed to be in daylight, and the difference between T_3

and T_4 assumed to be due to channel 3 reflected energy. For each of several values of solar zenith angle, the reflectivity was calculated for every point, and the percentage of points less than each reflectivity was determined. For the overwhelming majority of points, the error in reflectivity (the true reflectivity being zero) was only a few percent, unless the solar zenith angle was quite large. A solar zenith angle of 60° results in errors less than 6% for 95% of the points, while for a solar zenith angle of 80° the errors are much greater. A consideration of the effect of these errors on the final scene identification must be deferred until after a presentation of the method.

4. Method

This method was based on the reflectivities determined from channels 1, 2 and 3. Letting r_n be the reflectivity observed by channel n, three new quantities were defined:

$$\left.\begin{aligned} x &= \frac{r_1}{r_1 + r_2 + r_3} \\ y &= \frac{r_2}{r_1 + r_2 + r_3} \\ z &= \frac{r_3}{r_1 + r_2 + r_3} \end{aligned}\right\} \qquad (7)$$

such that $x + y + z = 1$. In addition, a mean reflectivity, $\bar{r}$, was calculated:

$$\bar{r} = \frac{r_1 + r_2 + r_3}{3} \qquad (8)$$

A central point was defined as $x = y = z = \frac{1}{3}$. The x-y-z coordinate system was transformed by determining the radial distance, d, in the x-y plane, from each observed x and y to the central point:

$$d = \sqrt{(x - 1/3)^2 + (y - 1/3)^2} \qquad (9)$$

and the angle, α, about the central point from the line 1/3,1/3:1/3,0 (the direction chosen for $\alpha = 0$ is arbitrary). It follows that

$$\sin\alpha = \frac{1/3 - x}{d} \quad , \quad \cos\alpha = \frac{1/3 - y}{d} \qquad (10)$$

x and y are both always positive, and from equation (7), $x+y \le 1$. For every value of α the radius d thus has a maximum value when x+y=1. In order to allow the radii at different angles to be compared directly, each observed radius was normalized by dividing by the maximum value for the corresponding angle: $D(\alpha) = d(\alpha)/d_{max}(\alpha)$. Letting the mean reflectivity, $\bar{r}$, be a third dimension orthogonal to the x-y plane (note that this is <u>not</u> the quantity z), a cylindrical coordinate system has been defined, with coordinates α, D, $\bar{r}$.

A series of observations of a perfectly homogeneous surface would necessarily all have the same values of α, D and $\bar{r}$, and would therefore appear as a single point. Natural surfaces, however homogeneous they may appear to the eye, will always display some degree of variability, and will therefore display a scatter of points in the α-D-$\bar{r}$ space. It is reasonable to assume that minor variations in a basically homogeneous surface will be distributed normally. Such a surface may thus be described by a trivariate normal distribution in α-D-$\bar{r}$ space. The .95 probability ellipsoid was adopted as defining that surface.

The size of the ellipsoid, in one or more dimensions, indicates the relative homogeneity of an observed surface. It is impossible to establish a general criterion of homogeneity, however, since some surface types (e.g., vegetation) are inherently more variable than others (e.g., extensive sand areas). As variability increases to a point where more than one surface type is involved, the assumption of normally distributed variations breaks down, and it is necessary to examine the distribution of observations directly. An attempt to fit such data using the assumption of normal distribution will result in an unrealistically large ellipsoid.

Based on images for channels 1 and 4, as well as general geographic information, a number of relatively small geographic areas were selected as representative of major catagories of surface type. Each area was sufficiently large to contain at least several hundred observations so that the computations are statistically significant. In the case of NOAA-6, where only channel 4 images were available, the channel 1 and 2 values were checked to insure that a low stratus situation was not mistakenly chosen as an example of clear conditions. A listing of the selected areas, with a brief statement of their characteristics, is given in Table 2. It must be stressed that no real ground truth was available for this data, and the choice of areas was thus dependent on a subjective evaluation of the available information. Consequently, there was no assurance that any area selected was truly homogeneous. A judgement could be made only *post facto*, by examining the sizes of the probability ellipsoids and the variability of the measurements in the various channels.

5. Results

It will be useful first to examine the variations which may occur with different illumination and viewing geometry.

In Fig. 5 are shown cross-sections of the probability ellipsoids for a desert surface and a water surface which were viewed on two successive orbits of NOAA-7. (Although all the 'desert' samples used in this study are true deserts, this term is defined properly as 'unvegetated land'. Thus, even a freshly plowed field would be included in this category). The two desert samples are located near $\alpha = 220^\circ$. The solid curves are for the case when the view was toward the sun, while for the dotted curves the view was away from the sun. For these desert surfaces the differences between the two situations is small, and in accordance with what is expected.

In the case of water, however, there is a drastic shift in the location, size, and shapes of the ellipsoids. The mean channel 4 temperature in both cases is about 290°K, with a narrow distribution. This would be expected, since the two sets of observations were taken only 100 minutes apart. Even if the channel 4 temperature is not the true water temperature, the error will be the same for both situations, and the results would be consistent. Further, the emissivity of water for channel 4 is .99925, and little error is made by assuming it to be equal to 1.

While the geometry when viewing toward the sun was such that the instrument could observe sunglint, it is evident from the magnitude of channels 1 and 2 data, as well as from the image, that a strong glint was not observed. Since T_3 was greater than T_4 for every observation in this sample, it appears that at least some of the solar energy reflected directly by the surface was seen by the satellite. However, the reflectivity of 0.01 which was calculated (using equation 4) appears too low. It is thus probable that much of the reflected radiation occurred at angles not viewed by the instrument.

When viewing a water surface away from the sun, no directly reflected radiation would be expected to be seen. That this is actually so is indicated by T_3 being less than T_4 for every observation in this sample. Consequently, equation 6 was used to estimate the reflectivity. For the solar zenith angle pertaining to this case, the expected reflectivity of a water surface is about 0.05. The calculated mean of 0.077 thus appears quite reasonable, with the excess probably being due to atmospheric effect. It may thus be concluded that the major shift in angle found when observing the same water surface with two viewing geometries is the result of the angular variation of reflection.

The differences resulting from the very different ranges of solar zenith angle observed by NOAA-6 and NOAA-7 cannot be examined for most surface types, since they may be expected to change significantly over such an extended period. The only surface type which may be assumed to remain constant is cloud-free desert (here referring to true desert, not merely temporarily unvegetated land). Fig. 6 shows probability ellipsoids for two Saharan areas that were observed from both satellites. Both areas are similar, being regions of extensive sand dunes. While the Calanscio Sand Sea showed only small changes betwen the observations, the Erg de Bilma showed a larger shift in angle and radius, although not nearly as great as was seen for water. The exact reason for the difference between the two areas is not known. However, it seems reasonable to assume that details of topography, surface constitution, etc., combined with differences in viewing geometry may be responsible, even though both are similar in overall type.

These examples are intended to illustrate the shift in parameters that may occur in different conditions even for the same surface. A detailed investigation of these changes could yield much information about the makeup of various surfaces and their patterns of reflection, but is beyond the scope of this study. As long as the major surface types can be separated clearly, variations within each type need not be considered.

Fig. 7 is a plot of probability ellipsoids for all areas listed in Table 2 for the catagories of vegetation, desert, water, and cloud. Since the radius proved not very useful in discriminating surface type, only the α-$\bar{r}$ dimension is shown. It may be seen that, in general, each surface type clusters more or less compactly. The reason for the wide variation in the parameters for water has already been discussed. Vegetation would be expected to exhibit a good deal of variability, owing to such factors as type of vegetation, state of growth, and amount of ground visible. Deserts are highly variable, as is evident from even a casual examination of a satellite image of e.g., the Sahara.

The cloud examples examined were similar in that they were all sufficiently extensive and bright and/or cold to be reasonably identified as homogeneous cloud. Within these constraints, however, they were selected from many parts of the geographic area available, both over land and over water. It is therefore interesting that clouds showed the tightest clustering of all the surface types.

The boundaries between pure scene types which were identified are shown in Fig. 7 as three straight lines. Any observation with a mean reflectivity greater than 39.6% is taken to be cloud. An observation to the left of the line $\bar{r} = 179.1 - 0.763\,\alpha$ is identified as vegetation. If the point lies to the right of this line and the satellite is viewing land, it is identified either as desert or as partial cloudiness, as will be discussed below.

The situation is the same for viewing over water. To the right of the line $\bar{r} = 2.5\,\alpha - 625$ lie values for clear water, while to the left are observations for partial cloudiness. As stated above, sunglint situations must be treated separately. For convenience of reference, these three lines will be termed the 'cloud boundary', the 'clear land boundary', and the 'clear water boundary', respectively.

Each surface type occupies a distinct region of the diagram, with two exceptions, both involving desert and water.

One water sample is quite large, and extends well into the region of desert. This sample was chosen as an example of very bright glint. It is simple to determine from the viewing geometry whether this situation is a possibility in any given case.

The second exception is a sample of very dark desert, some of the observations of which extend into the region which defines water. In such a case it would be impossible to decide on the basis of single observations what type of surface was being viewed.

Since the only major ambiguity found is between water and desert (and even then in only a small number of situations) the condition is simple to resolve. Land-water tags are appended to operational AVHRR GAC data. When these tags are applied to the present scene identification scheme, any ambiguity vanishes.

Ice and snow have not been included in Fig. 7, since their parameters are indistinguishable from those of clouds, due to the dominance of channels 1 and 2. Cloud and ice/snow are very similar in all channels except in channel 3. Fig. 8 shows frequency distributions for four cloud samples and one of ice. (It is very difficult to select areas of ice which are uncontaminated by clouds, precisely because they appear so similar). The clouds have a wide range of both distributions and reflectivities, due probably to variations in composition, illumination, and viewing geometry. However, not even a single cloud point has a reflectivity less than .01. For ice, almost all the values lie in the range 0 to .01. Those points which have greater value may very well result from cloud contamination. A value of the channel 3 reflectivity which is less than .01 would thus serve to distinguish ice from cloud.

It is now possible to assess the final effect on scene identification of the assumptions made regarding channel 3.

It may seen from equations 7, 9 and 10 that when $r_1 = r_2$, $\alpha = 225^\circ$, regardless of the value of r_3. It also may be seen from Fig. 7 that $\alpha = 225^\circ$ is approximately central to the scene distributions. Thus at this angle, any error in determining r_3 has no effect on the scene identification.

When $\alpha > 225^\circ$, increasing r_3 will cause α to increase, while the opposite is true when $\alpha < 225^\circ$. As a result, variations in r_3, while resulting in a shift of coordinates, will not be sufficient to change the identification of the scene type. This was verified by repeating the identification procedure for several areas, specifying for each a wide range of r_3, rather than the value calculated from the channel 3 observations. Only for very marginal situations did this result in a change of scene type.

How important, then, is channel 3 in the scene identification method? For separating snow or ice from cloud it is vital. For other scene types it serves in an auxilliary role, spreading the individual areas over a larger range of α

and thus permitting a more confident delimiting of scene type boundaries.

The major consideration, however, is whether the desired scene types can be separated satisfactorily. If this can be done, then the final algorithm and its parts, *as defined*, are successful, even if any part by itself is in error. Thus, although the channel 3 reflectivities obtained here are only approximately correct, their absolute accuracy is of secondary importance.

Usually the surface types in an observed area are mixed. It then cannot be assumed that any parameter is normally distributed, and it is necessary to examine the actual distribution of the observations. In practice, therefore, an array of observed points must be processed as a single batch. This procedure may be illustrated by considering three examples of mixed scenes: partial cloudiness over water, clear land ranging from vegetated to bare soil, and partial cloudiness over vegetation. The frequencies of occurence as a function of α and $\bar{r}$ for those areas are plotted in Figs. 9, 10 and 11 respectively.

The observations that represent homogeneous GAC views are first identified. Thus in Fig. 9 the three observations that have a reflectivity greater than 39.6% are identified as cloud, while those to the right of the clear water boundary are classified as water. The remaining observations, falling between these two groups represent various amounts of partial cloudiness. (Since it is assumed that a land-water discriminator is being used, there is no possibility of misidentifying any of these observations as desert.)

The interpretation of Fig. 10 is similar. The lack of reflectivities greater than 20% indicates that there are no clouds present in the area. The observations to the right of the clear land boundary are classified as desert, and those to the left as vegetation. However, the fact that the distribution is continuous indicates that the vegetation coverage differs from spot to spot.

The method of analysis of Fig. 11 is the same as for Fig. 9, except that here the major elements are vegetation and cloud. What is quite clear from this figure is the necessity of examining an array of observations, rather than attempting to classify each spot in isolation. Each partly cloudy spot examined individually could be misidentified as desert. Only after the overall context is determined from the distribution of values is it possible to specify the scene for individual GAC spots.

The observations in Figs. 9-11 come from relatively large geographical areas, and may include up to several thousand GAC spots. Such a size is computationally unwieldy, and tends to mask finer scale features. For routine processing a much smaller array is preferable. Since the operational processing of the AVHRR radiation budget uses an 11 x 11 array of GAC spots as its basic grouping, this would be a convenient size to use for scene identification.

Fig. 12 shows the distribution of observations for an

11x11 array selected arbitrarily from the data used to generate Fig. 11. Each of the 121 values is plotted individually. In an operational situation, the only *a priori* information would be that the satellite is viewing land. There are four observations which have reflectivites greater than 39.6%, and are therefore classified as totally cloud filled. A large number of points are to the left of the clear land boundary, and are identified as clear vegetation. Since there are present both cloud free and cloud filled pixels, the remaining observations are identified as partially cloud filled. Since in order to identify a scene as partly cloudy, it is necessary to have at least one pixel totally cloudy and one completely clear, this approach will yield a false result if all the pixels are partly cloudy.

In Fig. 12 there is present in this approximately 50 km square area a large variation in the parameters for clear vegetation. This may be attributed to such factors as vegetation type, degree of dryness, extent of ground cover, shadowing, etc. While such distinctions may be of interest to those interested in studying the nature and state of vegetative cover, it is of secondary importance for operational processing. It must, however, be considered when evaluating observations that are identified as partly cloudy. A curve describing the variation from clear to overcast would be expected to have the same form for each pixel. Due to variations of the underlying surface and of cloud properties, however, the particular constants will differ between pixels, giving rise to a family of curves.

The assumption was made that any individual curve will intersect both the clear land (or clear water) boundary and the cloud boundary at right angles. The curve shape was specified by requiring that the normal to the curve pass through the intersection point of the clear and cloud boundaries. To compute the cloud fraction for a partly cloudy pixel, a line is computed which passes through the α, $\bar{r}$ of the pixel and through the intersection of the pertinent clear and cloud boundaries. The angle between this line and the clear boundary, divided by the angle between the clear boundary and the cloud boundary yields the fractional cloudiness. The dashed lines in Fig. 12 are drawn for this ratio at intervals of 0.1. The total cloudiness computed for the observations shown in Fig. 12 is 18.3%.

6. Conclusion

The method presented here is capable of identifying for individual GAC spots major catagories of scene type: water, vegetation, desert, ice/snow, cloud and partial cloud. For a partly cloudy spot it can also estimate the cloud amount. Since the information required beyond the data for a single spot is already present in the operational processing, (i.e., 11 x 11 arrays and land-water discriminators), this method seems to be satisfactory as the basis for applying proper angular corrections for routine determination of the radiation budget. The incorporation of this method into the operational processing procedure and an evaluation of its accuracy in this context will be presented in a later document.

Table 2
Areas Used in Study
Homogeneous Areas

Name	Location	Type
Desert, NOAA-7		
Erg de Bilma	17-19°N,12-14°E	Erg (sand dunes)
Calanscio Sand Sea	28-29°N,23-25°E	Erg (sand dunes)
Hamada al Hamra	29-30°N,11.5-13.5°E	Hamada(rock plateau)
Ghadir ar Razzah	27-27.5°N,17-18°E	Dark Rock
Erg Chech	25-27°N,1-2°W	Erg (sand dunes), view toward sun
Erg Chech	25-27°N,1-2°W	Erg (sand dunes), view away from sun
Desert, NOAA-6		
Erg de Bilma	17-19°N,12-14°E	Erg (sand dunes)
Calanscio Sand Sea	28-29°N,23-25°E	Erg (sand dunes)
Tassili n'Ajjer	25-26°N,8-9°E	Dark hills (desert)
Tanezrouft	20-22°N,1-3°E	Reg(pebble pavement)
Vegetation, NOAA-7		
S. France	44-46°N,0-4°E	Vegetation
S. England	52-53°N,0-4°W	Vegetation
E. Brazil	18-20°S,42-43°W	Selva
Vegetation, NOAA-6		
E. Brazil	7-11°S,45-49°W	Wooded savanna and selva
Congo	0-2°N,19-21°E	Selva
Cent. African Rep.	6-8°N,18-21°E	Wooded savanna
Hungary	46-47°N,19-21°E	Vegetation
Water, NOAA-7		
Bay of Biscay	45-47°N,5-8°W	Water, view toward sun
Bay of Biscay	45-47°N,5-8°W	Water, view away from sun
Off C. of Good Hope	34.5-36°S,24-26°E	Water
30°N,46°W	29-31°N,45-47°W	Water
Balearic Sea	37-38°N,0-2°E	Water
Water, NOAA-6		
E. Mediterranean	23-24°N,31-33°E	Sunglint on water
1°S,30°W	0-2°S,29-31°W	Water
6°S,6°E	5-7°S,5-7°E	Water

Table 2, continued

Cloud, NOAA-7		
Greece	37-38°N, 21.8-22.8°E	Cloud
Bavaria	49-50°N, 10-13°E	Cloud
55°N, 35°W	54-56°N, 37-39°W	Cloud
35°S, 35°W	35-37°S, 35-37°W	Cloud
Cloud, NOAA-6		
46°N, 38°W	45-47°N, 37-39°W	Frontal cloud
42°S, 20°E	41-43°S, 18-22°E	Cloud
Congo	1.5-2.5°S, 25.5-26.5°E	Cloud
Ice, NOAA-7		
Greenland	76-79°N, 35-45°W	Ice

Mixed Areas
NOAA-7

Congo	2°S-2°N, 22-26°E	Part cloud over vegetation
10°S, 10°W	8-11°S, 8-12°W	Part cloud over water
N.W. Spain	39-42°N, 4-6°W	Vegetation, unvegetated land, mountains

References

Buettner, Konrad J.K. and Clifford D. Kern, 1965. The Determination of Infrared Emissivities of Terrestrial Surfaces. *Journal of Geophysical Research*, vol. 70, p. 1329.

Dana, Robert W., 1969: Measurements of 8 - 14 Micron Emissivity of Igneous Rock and Mineral Surfaces. *Scientific Report on Contract NASA NsG632*, Department of Atmospheric Sciences, University of Washington.

Gray, Thomas J. and Dee G. McCrary, 1981: The Environmental Vegetative Index: A Tool Potentially Useful for Arid Land Mangement. *Preprint Volume, 15th Conference on Agricultural and Forest Meteorology and Fifth Conference on Biometeorology*, A. M. S.

Rouse, J.W. Jr., R.H. Haas, J.A. Schell and D.W. Deering, 1974. Monitoring Vegetation Systems in the Great Plains with ERTS. *Third Earth Resources Technology Satellite-1 Symposium*, vol.1, sec. A, p. 309, N.A.S.A.

Suttles, J.T., R.N. Green, P. Minnis, G.L. Smith, W.F. Staylor, B.A. Wielicki, I.J. Walker, D.F. Young, V.R. Taylor and L.L. Stowe, 1988. Angular Radiation Models for the Earth-Atmosphere System. Part I: Shortwave Radiation. Langley Research Center, Hampton, Virginia, to be submitted for publication.

Wolfe, William L. and George J. Zissis, editors, 1978. *The Infrared Handbook*, Office of Naval Research, Washington, D.C.

Figure Captions

Figure 1. Relationship of LAC and GAC fields of view.

Figure 2. Normalized Spectral responses of AVHRR channels. Spectral distribution of incident solar energy at the top of the atmosphere and of energy emitted by a 300°K black body.

Figure 3. Solar zenith angle limit for calculating channel 3 reflectivity.

Figure 4. Channel 3 reflectivity as a function of temperature difference between channels 3 and 4 and channel 4 temperature. Solar zenith angle = 0°.

Figure 5. Probability ellipsoids for a desert surface and a water surface, each viewed at two different angles.

Figure 6. Probability ellipsoids for two desert surfaces viewed from both NOAA-6 and NOAA-7.

Figure 7. Probability ellipsoids for all homogeneous areas except ice.

Figure 8. Relative frequencies of occurence of channel 3 reflectivities for four cloud samples and one ice sample.

Figure 9. Plot of frequencies of occurence of combinations of angle and mean reflectivity for partial cloudiness over water.

Figure 10. Same as Fig. 9 for a mixture of vegetated and unvegetated land.

Figure 11. Same as Fig. 9 for partial cloudiness over vegetation.

Figure 12. Same as Fig. 9 for an 11 x 11 array selected from the data of Fig. 11.

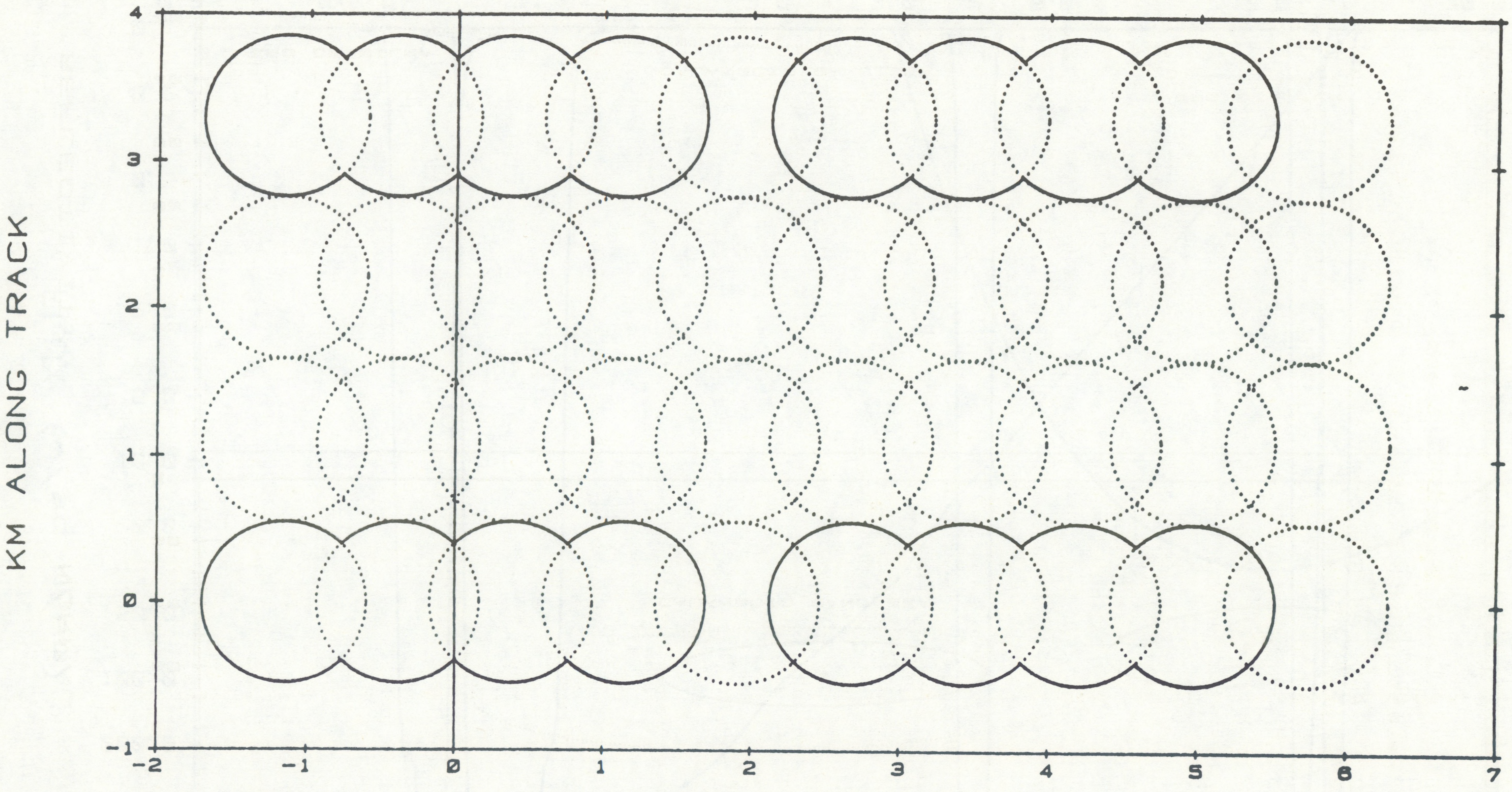

Fig. 1

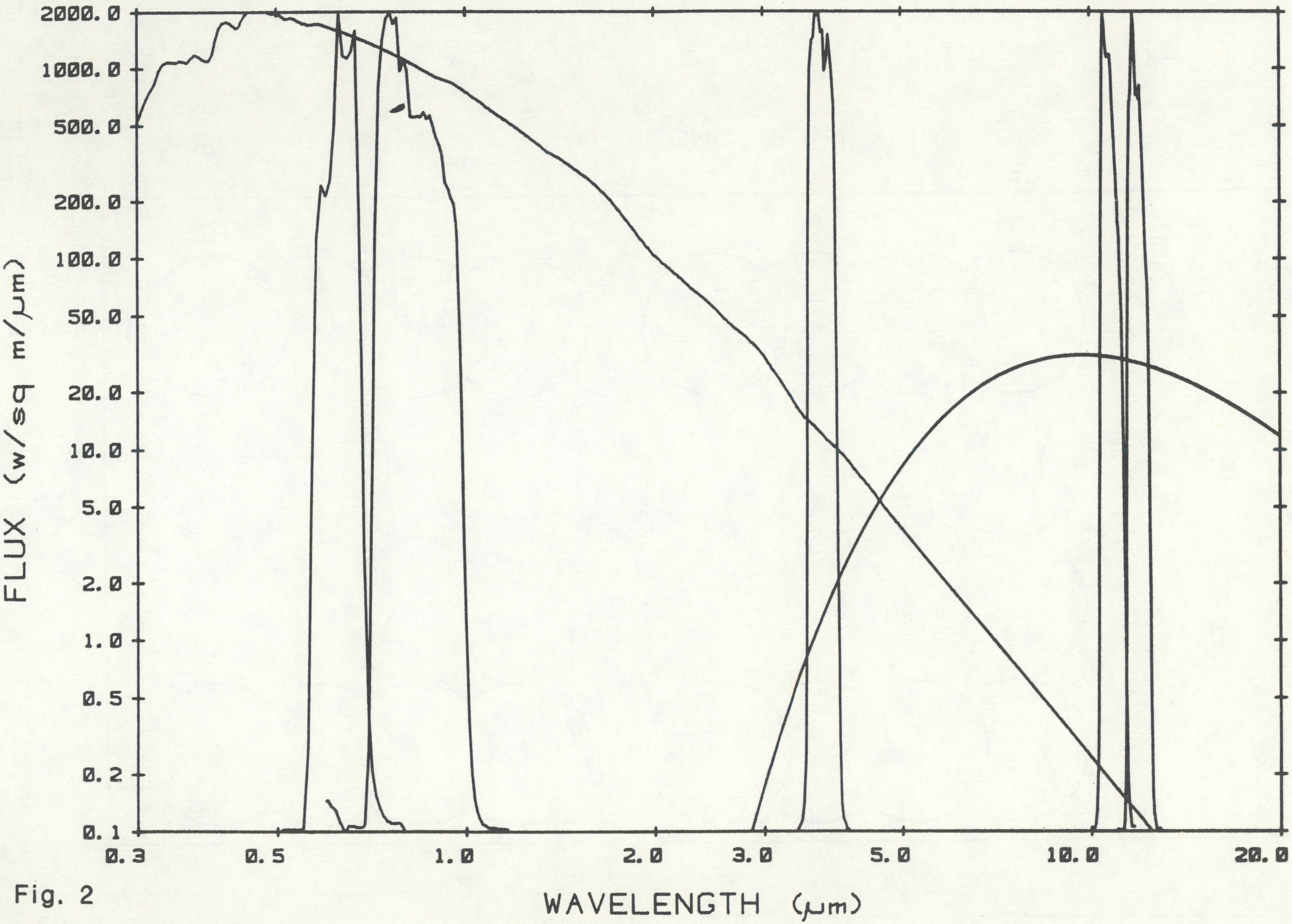
2000.0
1000.0
500.0
200.0
100.0
50.0
20.0
10.0
5.0
2.0
1.0
0.5
0.2
0.1
0.3
0.5
1.0
2.0
3.0
5.0
10.0
20.0
FLUX (w/sq m/μm)
WAVELENGTH (μm)

Fig. 2

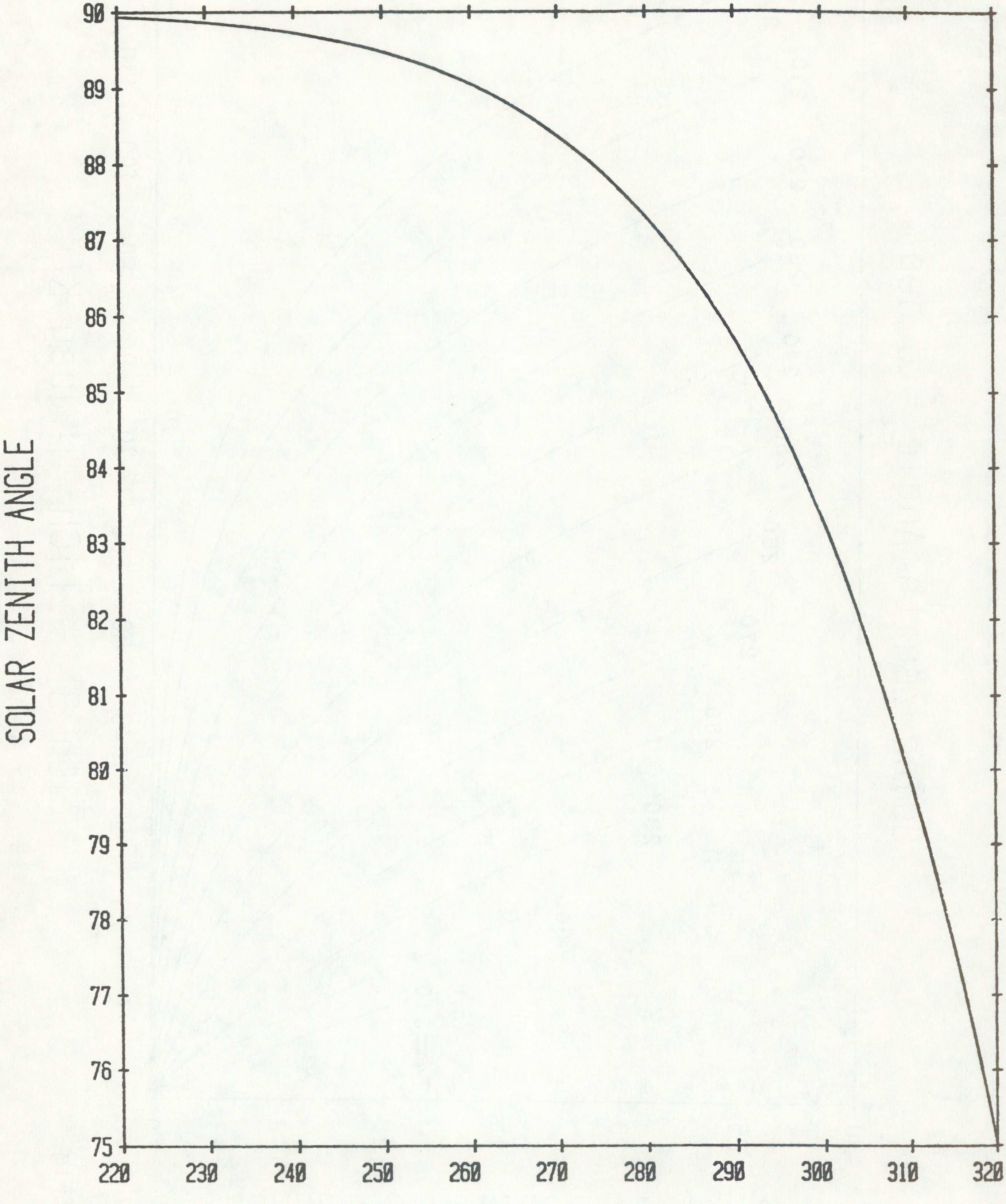
90
89
88
87
86
85
84
83
82
81
80
79
78
77
76
75
SOLAR ZENITH ANGLE
220
230
240
250
260
270
280
290
300
310
320
CHANNEL 4 TEMPERATURE (DEG K)

Fig. 3

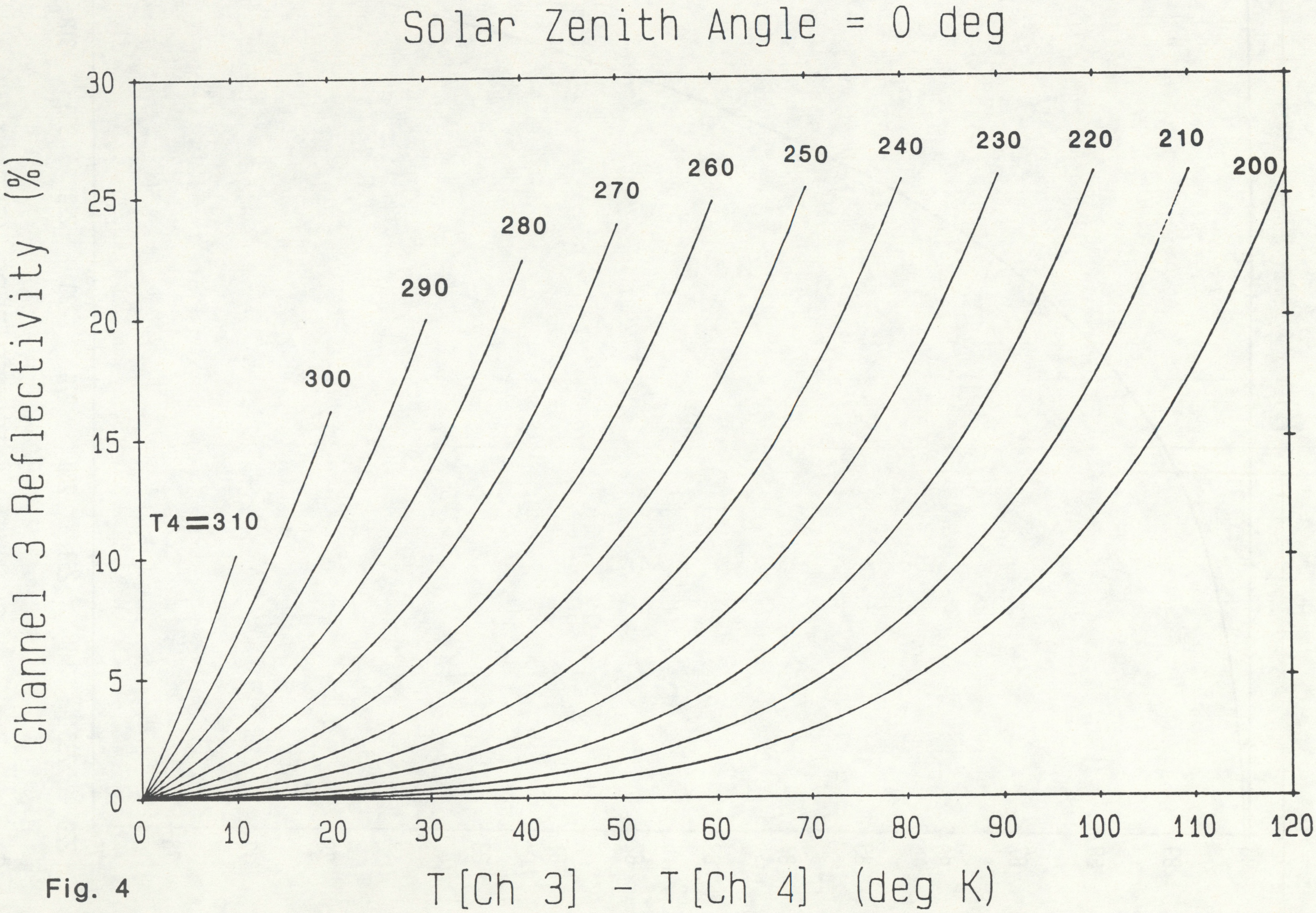

Solar Zenith Angle = 0 deg

Fig. 4

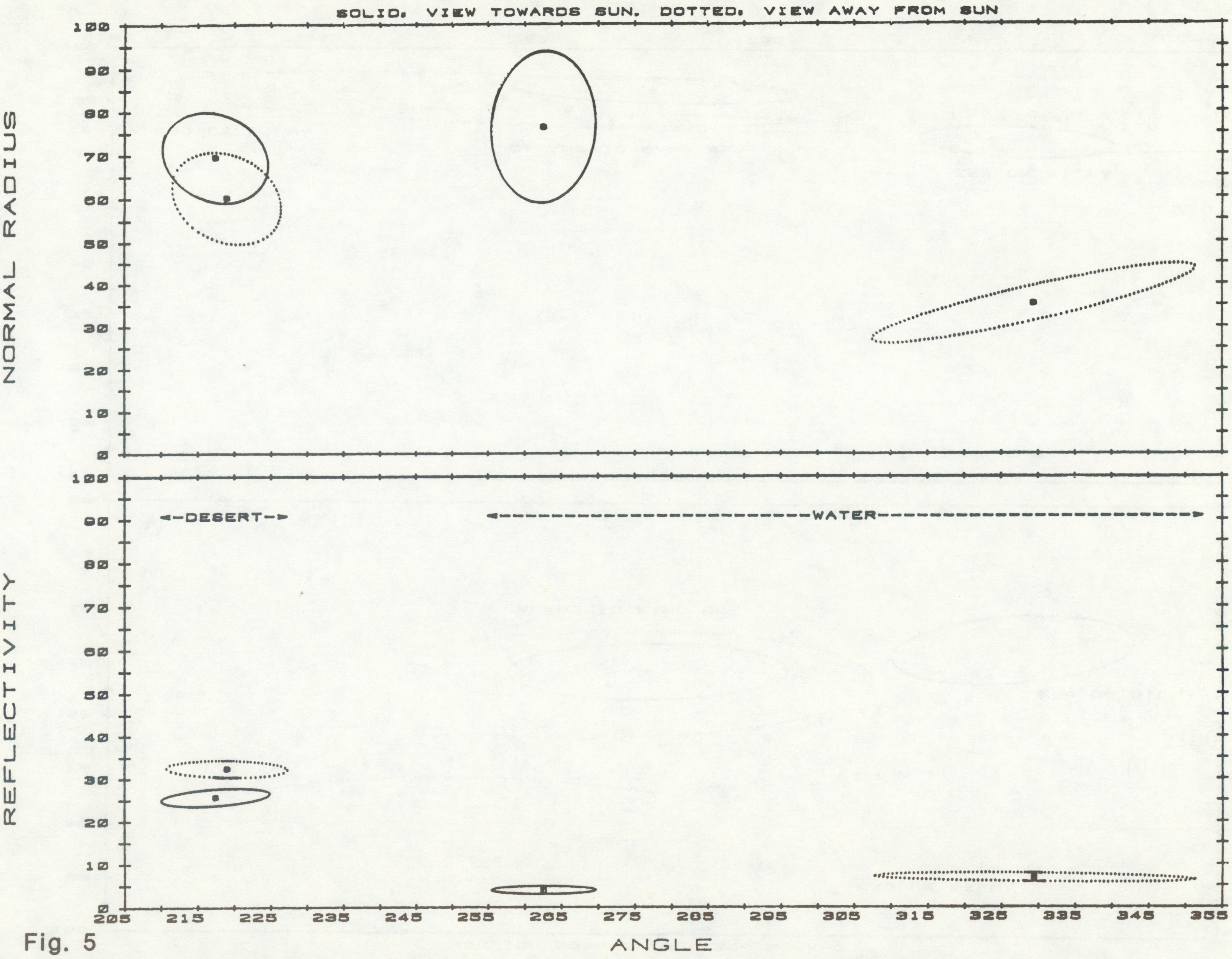
SOLID. VIEW TOWARDS SUN. DOTTED. VIEW AWAY FROM SUN
NORMAL RADIUS
100
90
80
70
60
50
40
30
20
10
0
REFLECTIVITY
100
90
80
70
60
50
40
30
20
10
0
<--DESERT-->
<-----WATER----->
205
215
225
235
245
255
265
275
285
295
305
315
325
335
345
355
ANGLE

Fig. 5

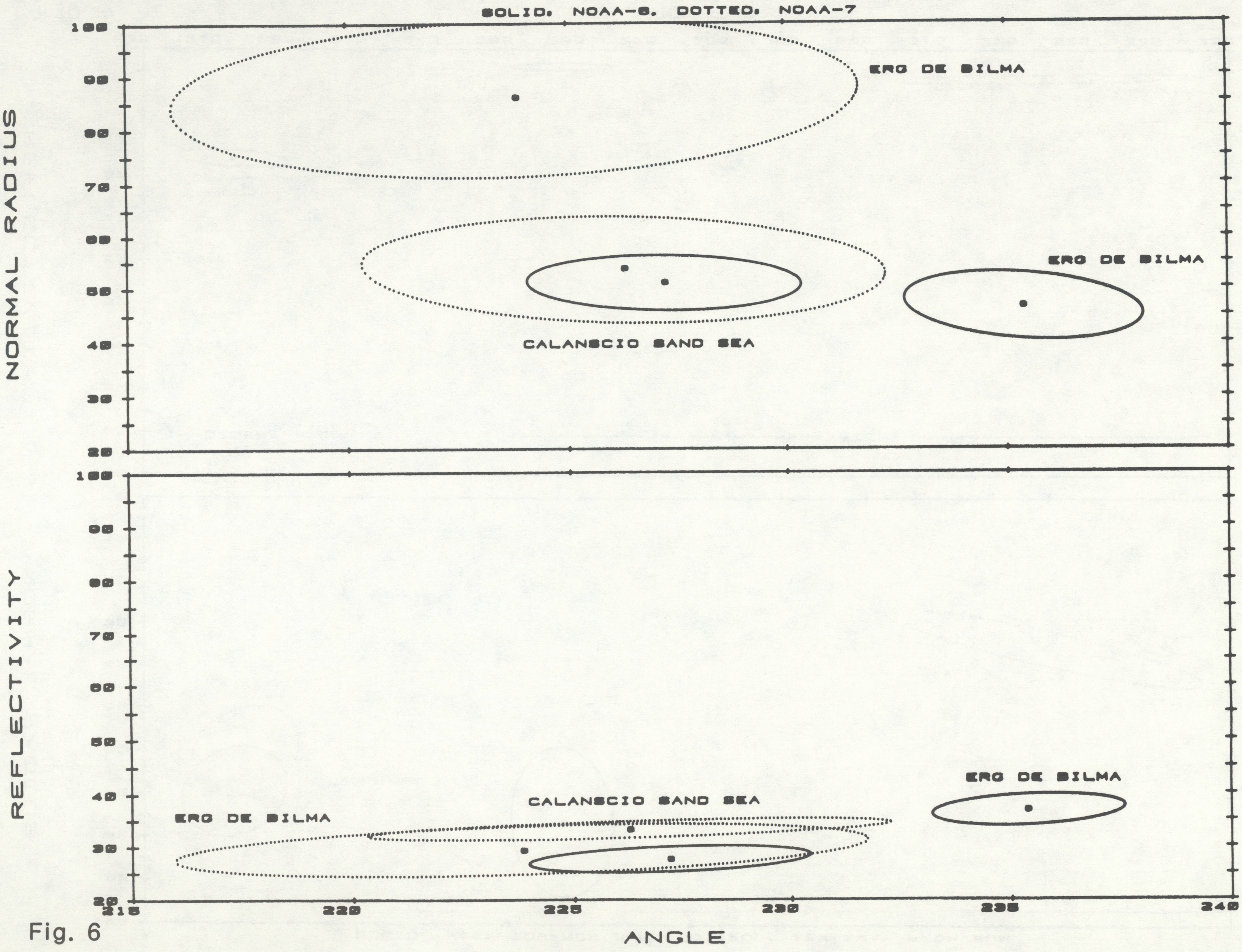
SOLID. NOAA-6. DOTTED. NOAA-7
NORMAL RADIUS
100
90
80
70
60
50
40
30
20
ERG DE BILMA
ERG DE BILMA
CALANSCIO SAND SEA
REFLECTIVITY
100
90
80
70
60
50
40
30
20
ERG DE BILMA
CALANSCIO SAND SEA
ERG DE BILMA
215
220
225
230
235
240
ANGLE

Fig. 6

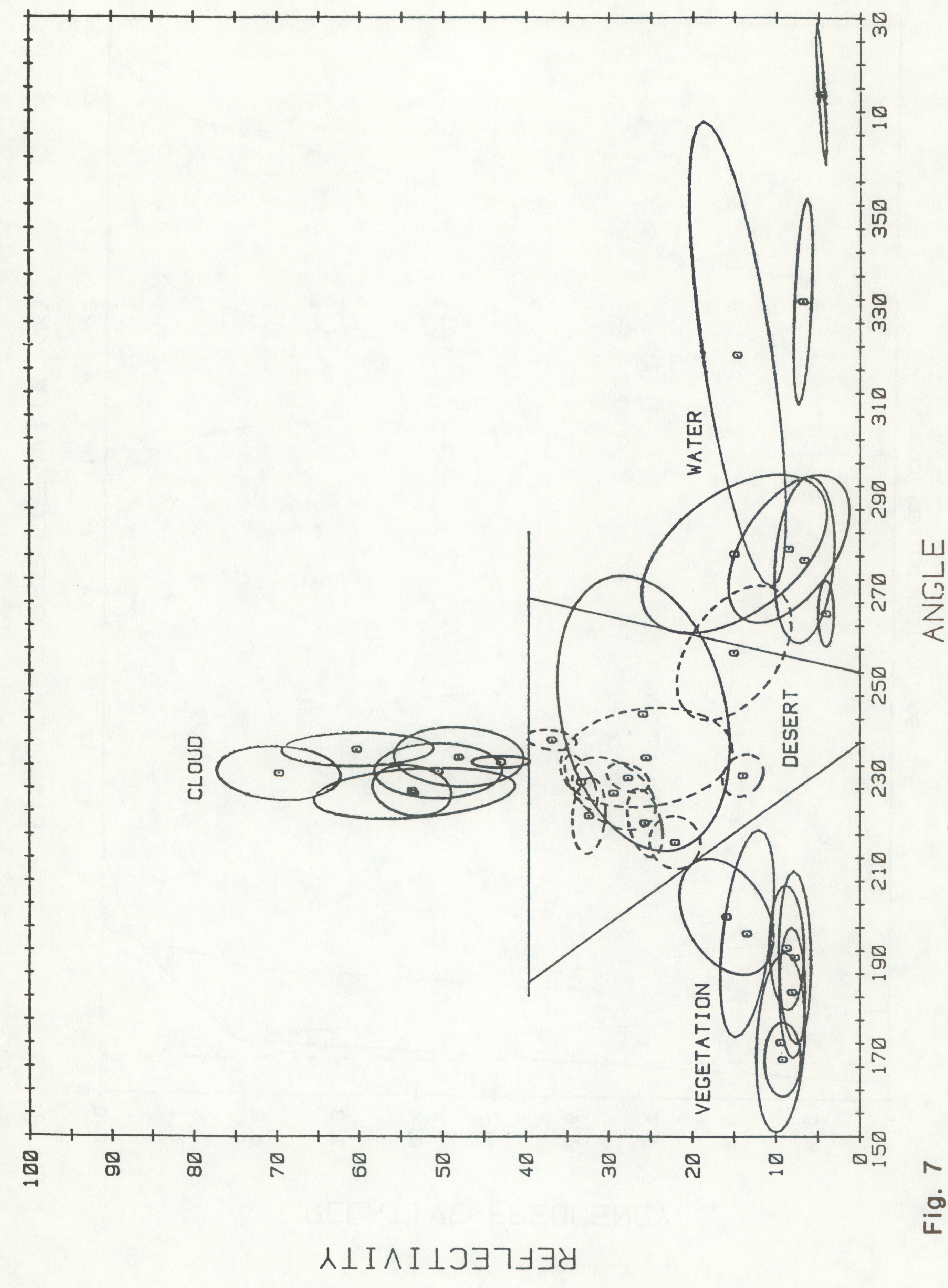
REFLECTIVITY
100
90
80
70
60
50
40
30
20
10
0
ANGLE
150
170
190
210
230
250
270
290
310
330
350
10
30
CLOUD
WATER
DESERT
VEGETATION

Fig. 7

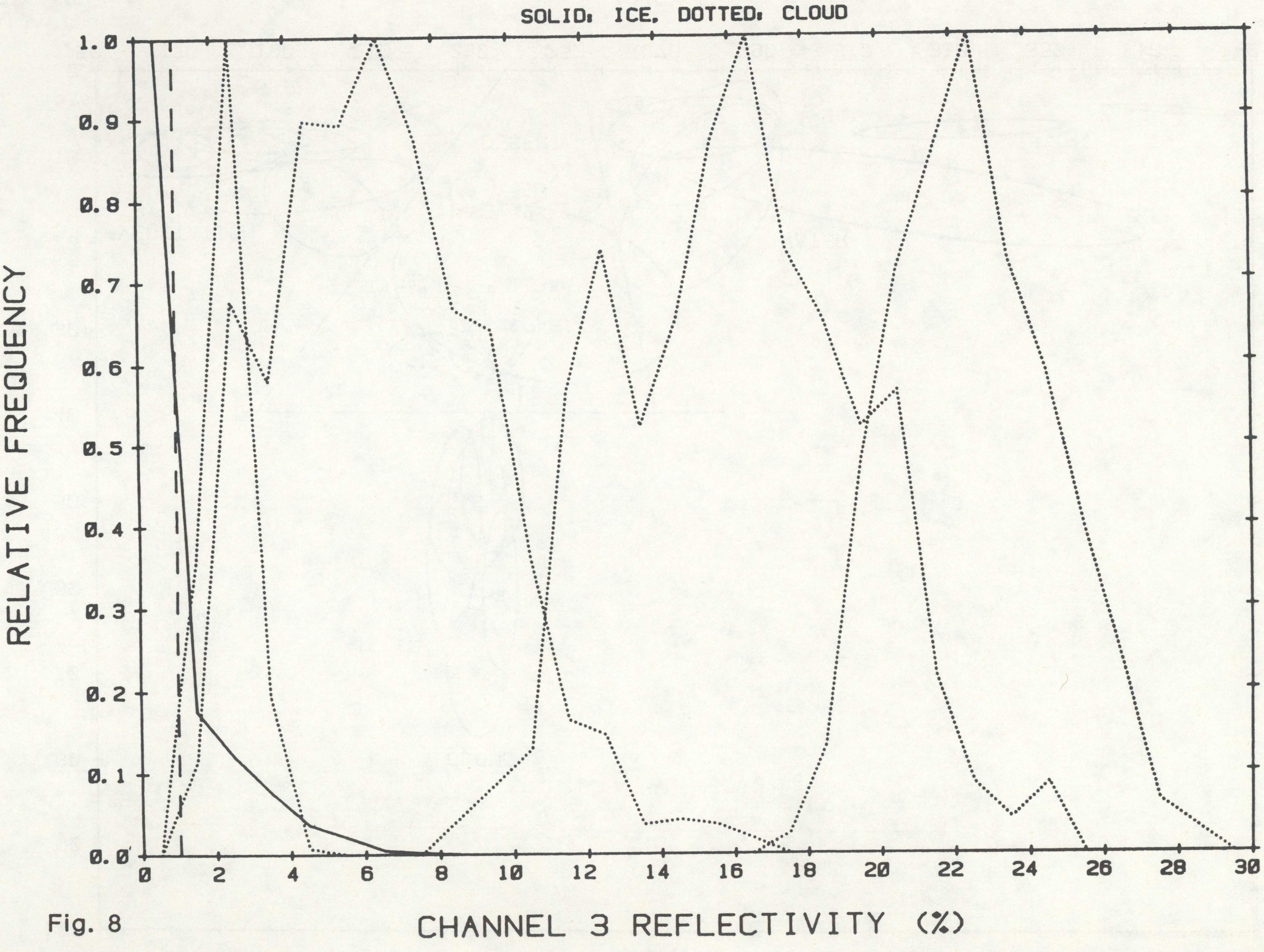
SOLID, ICE, DOTTED, CLOUD
RELATIVE FREQUENCY
1.0
0.9
0.8
0.7
0.6
0.5
0.4
0.3
0.2
0.1
0.0
0
2
4
6
8
10
12
14
16
18
20
22
24
26
28
30
CHANNEL 3 REFLECTIVITY (%)

Fig. 8

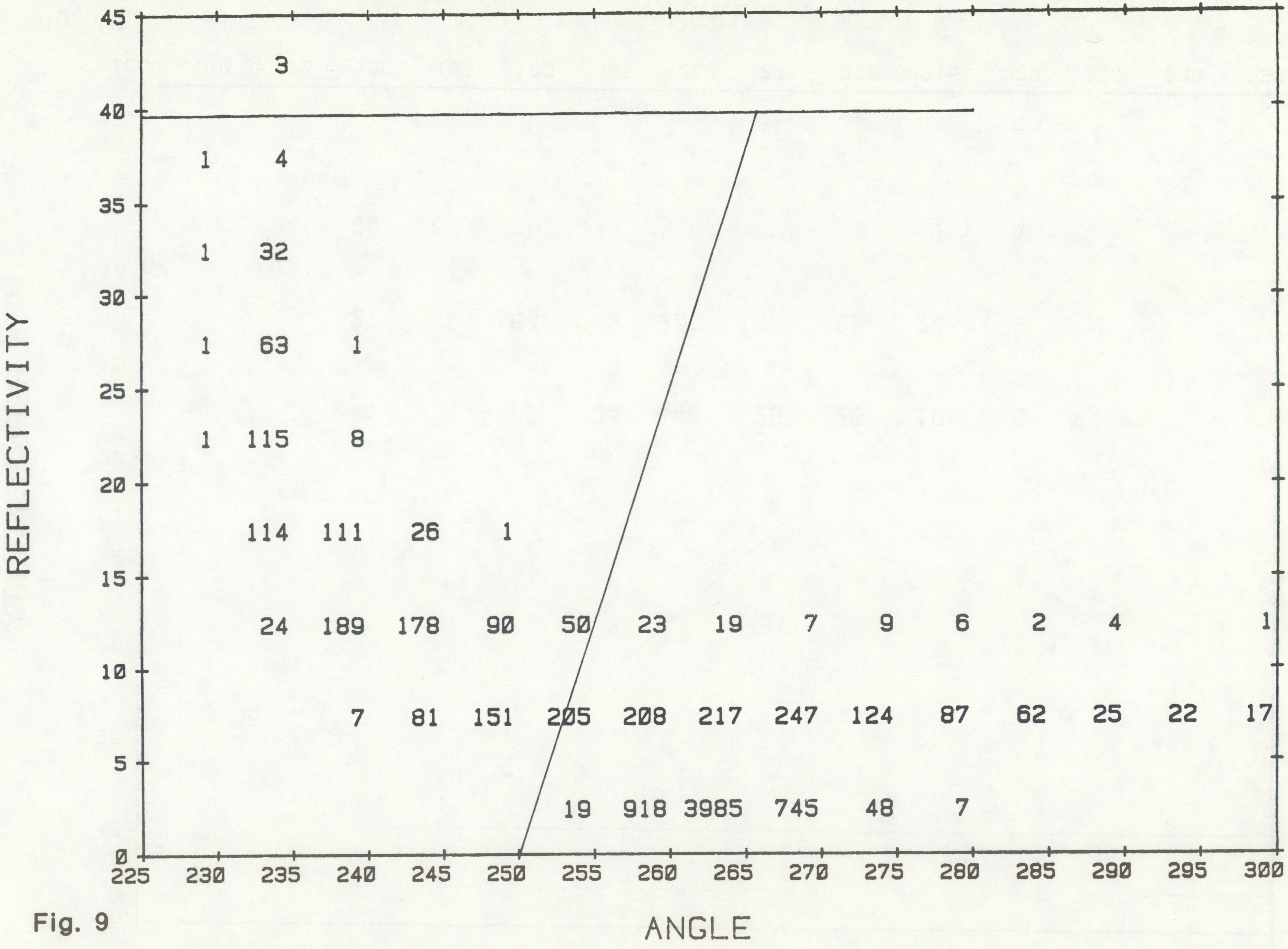
REFLECTIVITY
45
40
35
30
25
20
15
10
5
0
225
230
235
240
245
250
255
260
265
270
275
280
285
290
295
300
ANGLE
3
1 4
1 32
1 63 1
1 115 8
114 111 26 1
24 189 178 90 50 23 19 7 9 6 2 4 1
7 81 151 205 208 217 247 124 87 62 25 22 17
19 918 3985 745 48 7

Fig. 9

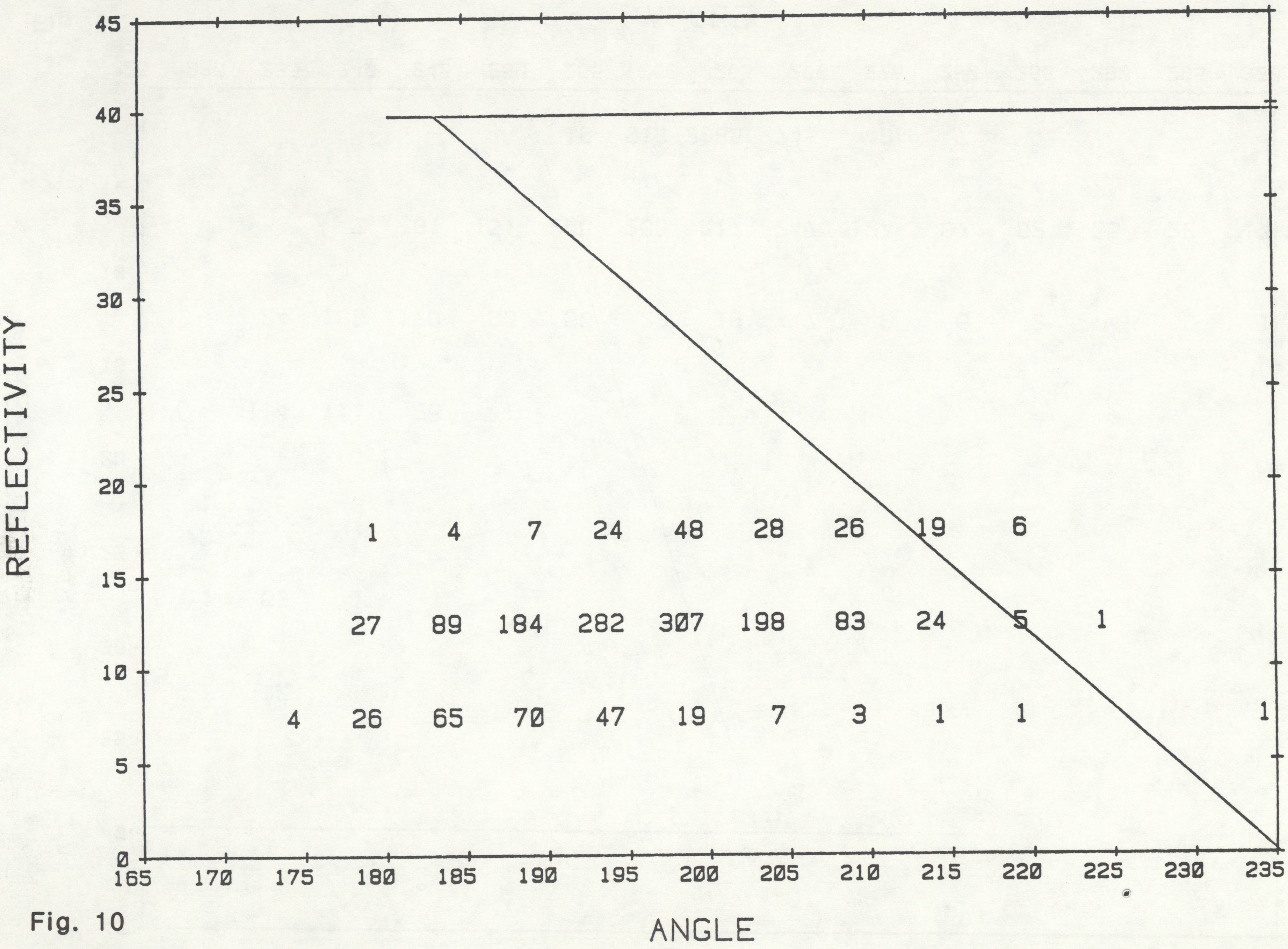
REFLECTIVITY
ANGLE
0
5
10
15
20
25
30
35
40
45
165
170
175
180
185
190
195
200
205
210
215
220
225
230
235
1 4 7 24 48 28 26 19 6
27 89 184 282 307 198 83 24 5 1
4 26 65 70 47 19 7 3 1 1 1

Fig. 10

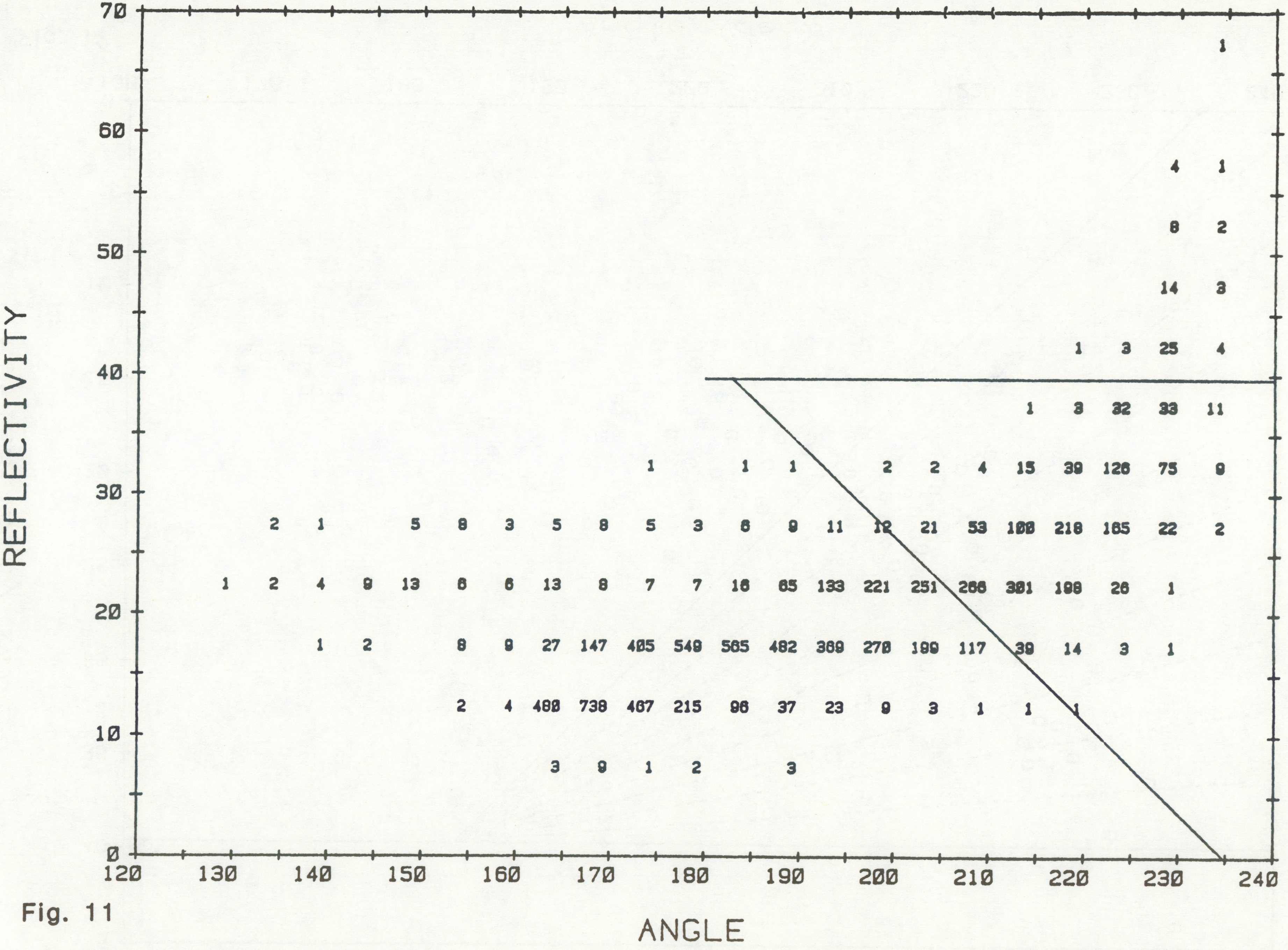
REFLECTIVITY
ANGLE
70
60
50
40
30
20
10
0
120
130
140
150
160
170
180
190
200
210
220
230
240
1
4 1
8 2
14 3
1 3 25 4
1 3 32 33 11
1 1 1 2 2 4 15 39 126 75 9
2 1 5 8 3 5 8 5 3 8 9 11 12 21 53 100 218 165 22 2
1 2 4 9 13 8 6 13 8 7 7 18 65 133 221 251 266 301 198 26 1
1 2 8 9 27 147 405 549 565 482 369 270 199 117 39 14 3 1
2 4 480 738 467 215 96 37 23 9 3 1 1 1
3 9 1 2 3

Fig. 11

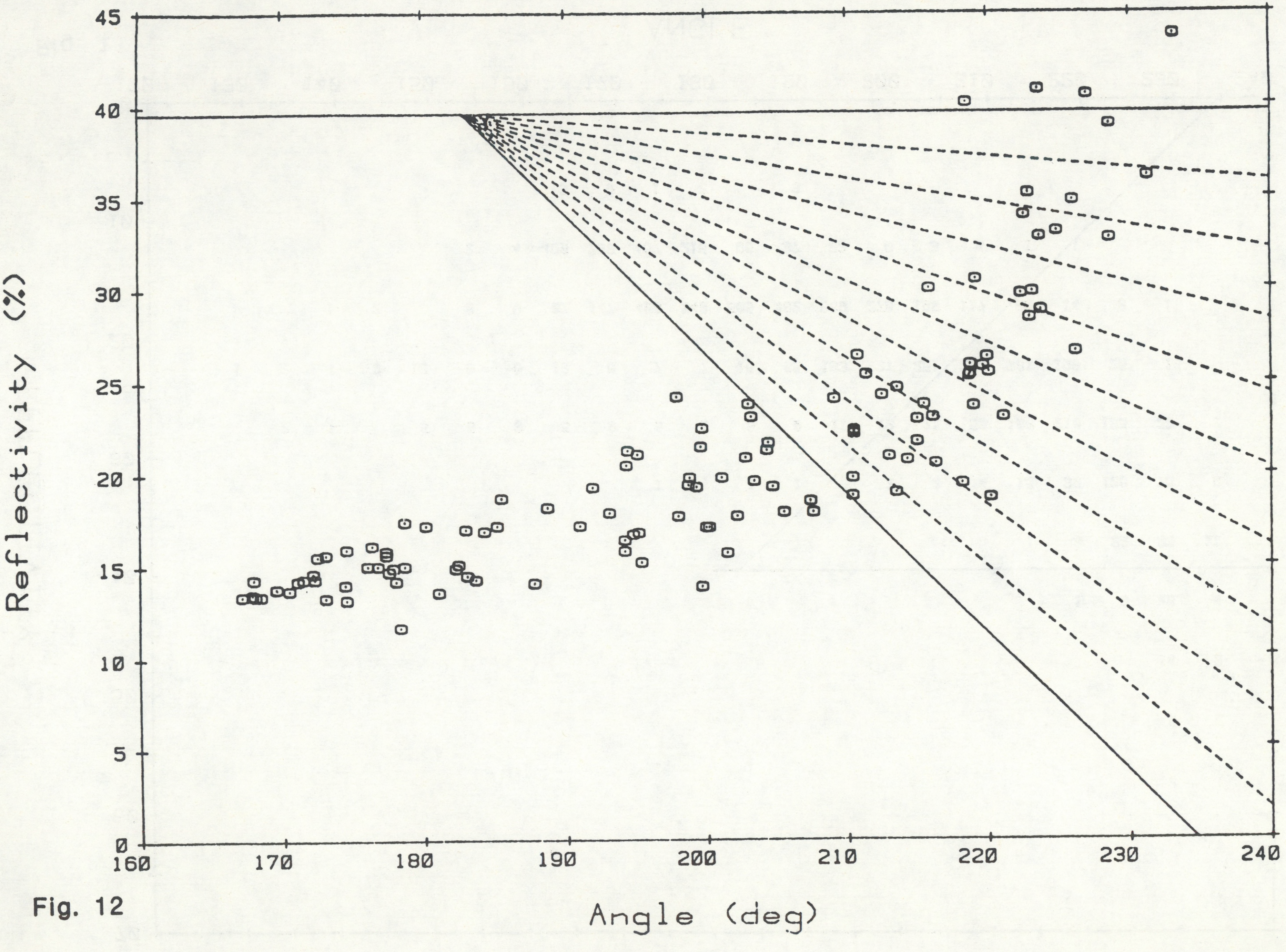
45
40
35
30
25
20
15
10
5
0
160
170
180
190
200
210
220
230
240
Reflectivity (%)
Angle (deg)

Fig. 12

(Continued from inside cover)

NESDIS 13 Summary and Analyses of the NOAA N-ROSS/ERS-1 Environmental Data Development Activity. John W. Sherman III, February 1984. (PB85 222743/43)

NESDIS 14 NOAA N-ROSS/ERS-1 Environmental Data Development (NNEEDD) Activity. John W. Sherman III, February 1985. (PB86 139284 A/S)

NESDIS 15 NOAA N-ROSS/ERS-1 Environmental Data Development (NNEEDD) Products and Services. Franklin E. Kniskern, February 1985, (PB86 213527/AS)

NESDIS 16 Temporal and Spatial Analyses of Civil Marine Satellite Requirements. Nancy J. Hooper and John W. Sherman III, February 1985. (PB86 212123/AS)

NESDIS 17 reserved

NESDIS 18 Earth Observations and the Polar Platform. John H. McElroy and Stanley R. Schneider, January 1985. (PB85 177624/AS)

NESDIS 19 The Space Station Polar Platform: Intergrating Research and Operational Missions. John H. McElroy and Stanley R. Schneider, January 1985. (PB85 195279/AS)

NESDIS 20 An Atlas of High Altitude Aircraft Measured Radiance of White Sands, New Mexico, in the 450-1050nm Band. Gilbert R. Smith, Robert H. Levin and John S. Knoll, April 1985. (PB85 204501/AS)

NESDIS 21 High Altitude Measured Radiance of White Sands, New Mexico, in the 400-2000nm Band Using a Filter Wedge Spectrometer. Gilbert R. Smith and Robert H. Levin, April 1985. (PB85 206084/AS)

NESDIS 22 The Space Station Polar Platform: NOAA Systems Considerations and Requirements. John H. McElroy and Stanley R. Schneider, June 1985. (PB86 6109246/AS)

NESDIS 23 The Use of TOMS Data in Evaluating and Improving the Total Ozone from TOVS Measurements. James H. Lienesch and Prabhat K.K. Pandey, July 1985. (PB86 108412/AS)

NESDIS 24 Satellite-Derived Moisture Profiles. Andrew Timchalk, April 1986. (PB86 232923/AS)

NESDIS 25 reserved

NESDIS 26 Monthly and Seasonal Mean Outgoing Longwave Radiation and Anomalies. Arnold Gruber, Marylin Varnadore, Phillip A. Arkin, and Jay S. Winston, October 1987. (PB87160545/AS)

NESDIS 27 Estimation of Broadband Planetary Albedo from Operational Narrowband Satellite Measurements. James Wydick, April 1987. (PB88-107644/AS)

NESDIS 28 The AVHRR/HIRS Operational Method for Satellite Based Sea Surface Temperature Determination. Charles Walton, March 1987. (PB88-107594/AS)

NESDIS 29 The Complementary Roles of Microwave and Infrared Instruments in Atmospheric Sounding. Larry McMillin, February 1987. (PB87 184917/AS)

NESDIS 30 Planning for Future Generational Sensors and Other Priorities. James C. Fischer, June 1987. (PB87 220802/AS)

NESDIS 31 Data Processing Algorithms for Inferring Stratospheric Gas Concentrations from Balloon-Based Solar Occultation Data. I-Lok Chang (American University) and Michael P. Weinreb, April 1987. (PB87 196424)

NESDIS 32 Reserved

NESDIS 33 An Introduction to the GOES I-M Imager and Sounder Instruments and the GVAR Retransmission Format. Raymond J. Komajda (Mitre Corp) and Keith McKenzie, October 1987, 47 pp.

NESDIS 34 Balloon-Based Infrared Solar Occultation Measurements of Stratospheric 03, H20, HNo3, and CF2C12. Michael P. Weinreb and I-Lok Chang (American University), September 1987, 27 pp.

NESDIS 35 Reserved

NESDIS 36 Pre-Launch Calibration of Channels 1 and 2 of the Advanced Very High Resolution Radiometer. C.R. Nagaraja Rao, October 1987, 62 pp.

NOAA SCIENTIFIC AND TECHNICAL PUBLICATIONS

The National Oceanic and Atmospheric Administration was established as part of the Department Commerce on October 3, 1970. The mission responsibilities of NOAA are to assess the socioeconomic impa of natural and technological changes in the environment and to monitor and predict the state of the soli Earth, the oceans and their living resources, the atmosphere, and the space environment of the Earth.

The major components of NOAA regularly produce various types of scientific and technical information in the following kinds of publications:

PROFESSIONAL PAPERS—Important definitive research results, major techniques, and special investigations.

CONTRACT AND GRANT REPORTS—Reports prepared by contractors or grantees under NOAA sponsorship.

ATLAS—Presentation of analyzed data generally in the form of maps showing distribution of rainfall, chemical and physical conditions of oceans and atmosphere, distribution of fishes and marine mammals, ionospheric conditions, etc.

TECHNICAL SERVICE PUBLICATIONS—Reports containing data, observations, instructions, etc. A partial listing includes data serials; prediction and outlook periodicals; technical manuals, training papers, planning reports, and information serials; and miscellaneous technical publications.

TECHNICAL REPORTS—Journal quality with extensive details, mathematical developments, or data listings.

TECHNICAL MEMORANDUMS—Reports of preliminary, partial, or negative research or technology results, interim instructions, and the like.

Stimulating America's Progress
1913-1988

U.S. DEPARTMENT OF COMMERCE
NATIONAL OCEANIC AND ATMOSPHERIC ADMINISTRATION
NATIONAL ENVIRONMENTAL SATELLITE, DATA, AND INFORMATION SERVICE
Washington, D.C. 20233